


# Structural determinants underlying the adduct lifetime in the LOV proteins of *Pseudomonas putida*

Vladimir Arinkin<sup>1,\*</sup>, Joachim Granzin<sup>1</sup>, Ulrich Krauss<sup>2,3</sup>, Karl-Erich Jaeger<sup>2,3</sup>, Dieter Willbold<sup>1,4,5</sup> and Renu Batra-Safferling<sup>1,4</sup> 

<sup>1</sup> IBI-7: Structural Biochemistry, Forschungszentrum Jülich, Germany

<sup>2</sup> Institut für Molekulare Enzymtechnologie, Heinrich-Heine-Universität Düsseldorf, Forschungszentrum Jülich GmbH, Germany

<sup>3</sup> IBG-1: Biotechnologie, Forschungszentrum Jülich GmbH, Germany

<sup>4</sup> Institut für Physikalische Biologie, Heinrich-Heine-Universität Düsseldorf, Germany

<sup>5</sup> Jülich Centre for Structural Biology (JuStruct), Forschungszentrum Jülich, Germany

## Keywords

adduct lifetime; crystal structure; dark recovery; LOV domain; PAS domain; photocycle; signaling

## Correspondence

R. Batra-Safferling, IBI-7: Structural Biochemistry, Forschungszentrum Jülich, D-52425 Jülich, Germany  
 Tel: +49-2461-619495  
 E-mail: r.batra-safferling@fz-juelich.de

## Present address

EMBL Heidelberg, Meyerhofstraße 1, Heidelberg, 69117, Germany

(Received 4 October 2020, revised 22 January 2021, accepted 22 February 2021)

doi:10.1111/febs.15785

The primary photochemistry is similar among the flavin-bound sensory domains of light–oxygen–voltage (LOV) photoreceptors, where upon blue-light illumination a covalent adduct is formed on the microseconds time scale between the flavin chromophore and a strictly conserved cysteine residue. In contrast, the adduct-state decay kinetics vary from seconds to days or longer. The molecular basis for this variation among structurally conserved LOV domains is not fully understood. Here, we selected PpSB2-LOV, a fast-cycling ( $\tau_{\text{rec}}$  3.5 min, 20 °C) short LOV protein from *Pseudomonas putida* that shares 67% sequence identity with a slow-cycling ( $\tau_{\text{rec}}$  2467 min, 20 °C) homologous protein PpSB1-LOV. Based on the crystal structure of the PpSB2-LOV in the dark state reported here, we used a comparative approach, in which we combined structure and sequence information with molecular dynamic (MD) simulations to address the mechanistic basis for the vastly different adduct-state lifetimes in the two homologous proteins. MD simulations pointed toward dynamically distinct structural region, which were subsequently targeted by site-directed mutagenesis of PpSB2-LOV, where we introduced single- and multisite substitutions exchanging them with the corresponding residues from PpSB1-LOV. Collectively, the data presented identify key amino acids on the A $\beta$ -B $\beta$ , E $\alpha$ -F $\alpha$  loops, and the F $\alpha$  helix, such as E27 and I66, that play a decisive role in determining the adduct lifetime. Our results additionally suggest a correlation between the solvent accessibility of the chromophore pocket and adduct-state lifetime. The presented results add to our understanding of LOV signaling and will have important implications in tuning the signaling behavior (on/off kinetics) of LOV-based optogenetic tools.

## Introduction

Light–oxygen–voltage (LOV) domains are a subset of the period (Per-), aryl hydrocarbon receptor nuclear translocator (Arnt), single-minded protein (Sim) (PAS) domain superfamily, which act as light-sensitive sensory domain in blue-light photoreceptors across multiple

kingdoms. Members of the LOV protein family play a role in controlling a number of cellular responses in plants, alga, fungi, archaea, and bacteria such as phototropism, chloroplast movement, stomatal opening, regulation of circadian rhythms, photo-induced growth

## Abbreviations

FMN, flavin mononucleotide; LOV, light–oxygen–voltage; PAS, Per-ARNT-Sim; Pp, *Pseudomonas putida*; RBF, riboflavin.

patterns and photosynthesis pigment synthesis, general stress responses, gene expression, and virulence [1–3]. Structurally well conserved, LOV domains display an overall  $\alpha + \beta$ -fold of PAS topology, where the core domain is composed of  $\sim 110$  residues. LOV domains are usually present in multidomain proteins that contain at least one effector domain in addition to at most two LOV domains. Additionally, a number of LOV domains have been identified as stand-alone single full-length photoreceptor proteins, lacking any additional effector domains [3–8]. According to a recent survey, about 16% of the known LOV photoreceptors are such short LOV proteins, which renders them the third largest LOV protein subfamily [4]. At present, the physiological role of these short LOV proteins is poorly understood and is known only for a few members. For example, VVD, a short LOV protein in fungi, functions as an antagonist of White Collar-1 (WC-1) complex, triggering a multitude of light responses [9]. Another short LOV protein, DsLOV from a marine phototrophic bacterium, plays a regulatory role in the induction of photopigment synthesis [3]. The RsLOV protein from purple photosynthetic bacteria not only affects blue-light-dependent gene expression but also plays a role in redox-dependent regulation [8,10]. Very recently, the physiological function of the two short LOV photoreceptors, PpSB1-LOV and PpSB2-LOV, of the saprotrophic soil bacterium *Pseudomonas putida* KT2440 was revealed [11]. The two short LOV photoreceptors, together with three homologs of class II LitR/CarH family of adenosyl B<sub>12</sub> (AdoB<sub>12</sub>)-dependent light-sensitive MerR transcriptional regulators (designated as PplR1–PplR3), regulate the light-inducible expression of a number of genes such as DNA-photolyases, the furan-containing fatty acid synthase *folE*, a GTP cyclohydrolase I, a cryptochrome-like protein, and various genes of unknown function. Since class II LitR/CarH proteins do not fully retain the domains responsible for AdoB<sub>12</sub> binding of class I LitR/CarH proteins, and light-inducible gene expression was independent of B<sub>12</sub> biosynthesis in *P. putida* [11], one can speculate that the two short PpSB-LOV proteins serve as (protein–protein interaction dependent) light-input modules for the three PplRs. The two proteins would thereby modulate the repressor function of PplR and cooperatively regulate the transcription of the light-inducible genes.

For light sensing, all LOV domains rely on blue-light absorbing flavin chromophores such as flavin mononucleotide (FMN) [or sometimes flavin adenine dinucleotide (FAD) and rarely riboflavin (RBF)], which are noncovalently bound within the LOV domain in the dark. Blue-light absorption by the LOV domains flavin chromophore essentially leads to the

formation of a covalent adduct between the flavin and a strictly conserved cysteine residue in the time range of  $\sim 200$  ns to 2  $\mu$ s [12–16]. This conformational state of the protein is referred to as the light state, which is stable over a wide range of time scales among different LOV proteins, varying from seconds to days [3,6,7,17–21]. As illumination ceases, the FMN–Cys adduct is thermally broken and the initial dark state is recovered at a characteristic time constant often reported as the adduct-state lifetime. Both, our group and others have published high-resolution structures of short LOV proteins in the light and dark states, providing insight on the light-induced signaling mechanism [19,22–26]. However, even high-resolution 3D structures have not explained the reasons for the variation in observed adduct-state lifetimes among structurally similar LOV domains.

In this study, we aimed to gain insight into the factors that determine adduct-state decay in the fast-cycling PpSB2-LOV protein using a comparative approach. For this, we determined the crystal structure of PpSB2-LOV in the dark state which shows high similarity to our previously published structures of PpSB1-LOV [6,22], prompting us to perform a sequence-based structural comparison of the two proteins. Based on the crystal structures, we performed molecular dynamic (MD) simulations to identify structural regions that exhibit altered flexibility in the light and dark states of the two proteins, and reasoned that these differences could partly account for the differences in adduct-state decay. Combining the structure information, sequence comparison, and MD simulation studies, selected residues in those regions were targeted by site-directed mutagenesis. To probe single-site and multisite combinatorial effects, we exchanged one to six residues in PpSB2-LOV with the corresponding residues from PpSB1-LOV and studied the functional consequences of those mutations on the adduct-state lifetime. Collectively, our data identify key residues located in the A $\beta$ –B $\beta$ , E $\alpha$ –F $\alpha$  loops, and the F $\alpha$  helix, which together with known residues such as H61 and I66 affect the adduct-state lifetime in a cooperative fashion. In addition, a correlation is found between the adduct-state lifetime and the size of solvent-accessible cavities.

## Results

To understand the molecular basis for the large variation in adduct-state lifetime and hence the dark recovery kinetics in the homologous short LOV proteins PpSB2-LOV and PpSB1-LOV, we applied a combined approach where in the first part, we investigated the crystal structure of the PpSB2-LOV protein. Structures

of PpSB1-LOV were previously reported by our group in the dark as well as in fully light-adapted states [6,22]. In the second part, we compared the structures and sequences of both the proteins and performed MD simulation studies. Based on the comparative analysis, in the third part, we selected residues for site-directed mutagenesis and determined the adduct-state lifetime of the resulting PpSB2-LOV mutants, where selected residues were exchanged with the corresponding residues from PpSB1-LOV.

### Purification and crystallization in the dark state

The recombinant PpSB2-LOV protein was expressed and purified from *Escherichia coli*. As quality indicators, flavin chromophore loading and composition were quantified for the immobilized metal affinity chromatography (IMAC) purified protein. The chromophore composition of the purified PpSB2-LOV protein was determined as 70% FMN, 21.3% RBF, and 8.7% FAD, which is in excellent agreement with previously reported values of 70% FMN, 26% RBF, and 4% FAD [6,7]. After *in vitro* loading, the FMN content increased up to 99.0%. Homogeneous chromophore content is important for structural and biochemical studies as variation in the type of incorporated flavin chromophore may result in alteration of the adduct-state lifetimes [17,27].

The PpSB2-LOV crystallization trials were performed under dark as well as under permanent blue-light (465 nm) illumination. Only crystallization in the dark conditions produced crystals suitable for diffraction experiments. Failure to crystallize the protein under blue-light illumination may be related to the short adduct-state lifetime of 3.5 min at 20 °C, which

does not allow for a kinetically stable, homogeneous population of molecules in the light state, but is required for the formation of an ordered crystal.

The UV-Vis spectra of dark grown PpSB2-LOV crystals cooled to 100 K were similar to the dark-state spectrum of PpSB2-LOV in solution at 293 K, indicating the preservation of dark state in cryocooled crystals (Fig. 1).

### Structure of the PpSB2-LOV dimer in the dark state

The crystal structure of PpSB2-LOV in the dark state was determined at a resolution of 1.93 Å in the monoclinic space group P2<sub>1</sub>. The data collection and refinement statistics are listed in Table 1. The asymmetric unit contains a homodimer, formed by monomers with a noncrystallographic twofold symmetry (Fig. 2A). Each monomer has a bound FMN chromophore. From a total of 148 residues, all residues in the electron density map could be traced in chains A and B. One of the residues from the N-terminal expression-tag observed in chain A was numbered 0. Superposition of monomers in Fig. 2B shows their overall similarity, with the RMSD of 0.72 Å for the C $\alpha$  atom positions for residues 1–145. The only differences between the monomers were in the loop regions: A $\beta$ -B $\beta$ , E $\alpha$ -F $\alpha$ , and H $\beta$ -I $\beta$ , likely induced due to crystal packing (Fig. S1).

The PISA analysis [28] of the dimer present in the crystal structure revealed a calculated total buried surface area of 3390 Å<sup>2</sup> with a −28 kcal·mol<sup>−1</sup> solvation energy gain upon dimer formation, indicative of a stable dimer in solution. The dimer interface is stabilized by hydrophobic interactions as well by hydrogen bonds

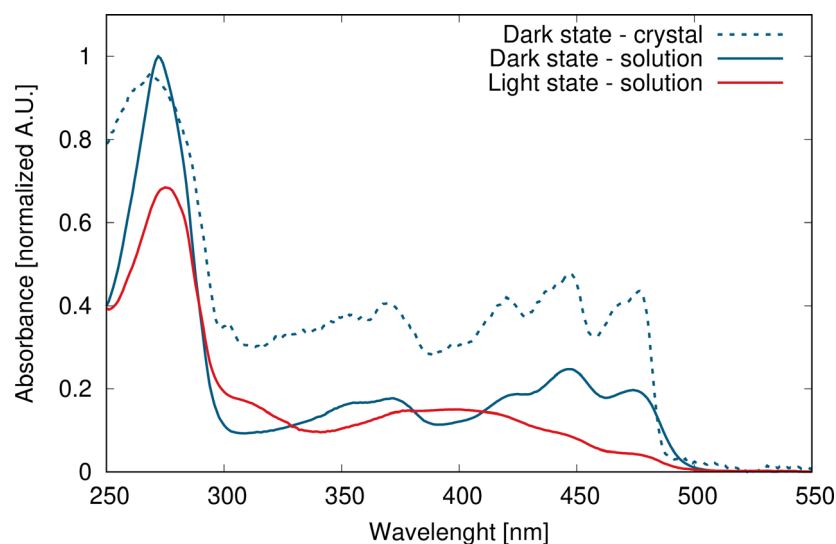


**Fig. 1.** UV-Vis spectra of PpSB2-LOV in solution and in crystal. PpSB2-LOV UV-Vis spectra in the dark and light states, measured both in solution (solid lines) and of the crystal grown in the dark (dashed line). Spectra were plotted with the Gnuplot program [66].

**Table 1.** Data collection and refinement statistics of PpSB2-LOV crystal structure. Statistics for the highest resolution shell are shown in parentheses.

X-ray Data	PpSB2-LOV (dark state) PDB ID: 7A6P
Beamline/Detector	ID23-2, ESRF Grenoble/ DECTRIS PILATUS3 X 2M
Wavelength (Å)/ Monochromator	$\lambda = 0.8726$
Resolution range (Å)	44.88–1.93 (1.98–1.93)
Space group	P 2 <sub>1</sub>
Unit cell <i>a</i> , <i>b</i> , <i>c</i> (Å); $\alpha$ , $\beta$ , $\gamma$ (°)	37.14, 88.47, 54.18; 90.0, 106.03, 90.0
Total reflections	107 111 (6856)
Unique reflections	25 353 (1705)
Multiplicity	4.2 (4.0)
Completeness (%)	100.0 (100.0)
Mean <i>I</i> /sigma( <i>I</i> )	8.9 (1.4)
Wilson <i>B</i> -factor (Å <sup>2</sup> )	29.14
<i>R</i> -merge	0.097 (0.890)
<i>R</i> -meas	0.111 (1.028)
Mn(I) half-set correlation CC(1/2)	0.997 (0.450)
Refinement	
Resolution range (Å)	44.88–1.93 (1.999–1.93)
<i>R</i> -work	0.1769 (0.2711)
<i>R</i> -free	0.1944 (0.3319)
Coordinate error (max.-likelihood based)	0.23
Number of nonhydrogen atoms	2530
Macromolecules	2375
Ligands	73
Water	82
Protein residues	299
RMS (bonds / angles)	0.008 / 0.91
Ramachandran favored (%)	98.7
Ramachandran outliers (%)	0
Clashscore	2.93
Average <i>B</i> -factor (Å <sup>2</sup> )	39.18
Macromolecules (Å <sup>2</sup> )	39.28
Ligands (Å <sup>2</sup> )	34.45
Solvent (Å <sup>2</sup> )	40.51
Number of TLS groups	9

and salt bridges. Interfacial residues are predominantly situated in the A'α helix, the Jα helix, and spread throughout the β-scaffold of core domain (Table 2).

The overall fold of PpSB2-LOV is α + β-fold of PAS topology, similar to the crystal structure of PpSB1-LOV in the dark state [22], where the conserved core domain comprises residues 17–118. Additionally, two non-canonical structure elements are present that protrude away from the LOV core domain: N-terminal helix A'α (residues 3–12) and long C-terminal helix Jα (residues 120–145), as previously observed in other LOV proteins from *Pseudomonas* species [6,17,22].

## Chromophore pocket

Light–oxygen–voltage proteins can generally accept RBF, FMN, and FAD as a chromophore [17]. The FMN chromophore is tightly coordinated by amino acids with total buried surface area of ~ 850 Å<sup>2</sup>. Similar to PpSB1-LOV and other LOV domains, residues involved in FMN coordination are mainly spread over the β-strands: Gβ, Hβ and Iβ, and α-helices: Eα and Fα (Fig. 3A,B). The adduct-forming C53 residue of PpSB2-LOV adopts two conformations with occupancies of 0.49/0.51 for chain A. Also, for chain B there are indications that a minor fraction of C53 adopts a second conformation. Two dark-state conformations for the adduct-forming cysteine residue have been previously reported in other dark-state LOV structures [29–33].

## Comparison to PpSB1-LOV

As mentioned above, PpSB2-LOV and PpSB1-LOV are two homologous proteins with sequence identity of ~ 67% from the same strain of *P. putida* [7]. Most differences in the amino acid sequences are localized in the Fα and Jα helices (Fig. 3B). Additionally, the C-terminal Jα helices of PpSB2-LOV are twelve residues longer as first, the PpSB1-LOV sequence is six residues shorter, and second, the C-terminal six residues are disordered in the crystal structure. The Jα coiled-coil interactions are largely hydrophobic in nature with a unique set of salt-bridge interactions between E135 and R140 of the noncrystallographic-symmetry-related monomers of the dimer (Table 2).

## Molecular dynamic simulation shows differences in dynamics of PpSB2-LOV and PpSB1-LOV

In order to investigate dynamics of PpSB2-LOV and its possible influence on adduct lifetime, we performed MD simulations of PpSB2-LOV and PpSB1-LOV in the dark states for 100 ns (two times 50 ns). Their respective crystal structures were used as the initial models. Overall, the structures remained stable over the course of the simulation (Fig. S2). The root-mean-square fluctuation (RMSF) of the core domain residues 17–119 of PpSB2-LOV and PpSB1-LOV was calculated and is presented in Fig. 4A. The overall RMSF of main chain atoms (N, Cα, C, and O) showed some increase in dynamics in PpSB2-LOV, with the most pronounced changes observed for the Aβ-Bβ and Hβ-Iβ loops, and regions including Cα, Dα, Gβ, and Hβ.

Comparison of side chain RMSF values showed that some of the discrepancies maybe related to the

**Fig. 2.** Crystal structure of the PpSB2-LOV in the dark state. (A) The structure is represented as ribbons, where chains A and B are colored in green and blue. FMN is shown as a stick model and is colored by element: carbon—yellow; nitrogen—blue; oxygen—red; phosphorus—pink. (B) Superposition of the two protein chains. The RMSD of the C $\alpha$  atom positions is 0.72 Å. Figures shown were generated with the UCSF Chimera software [62].

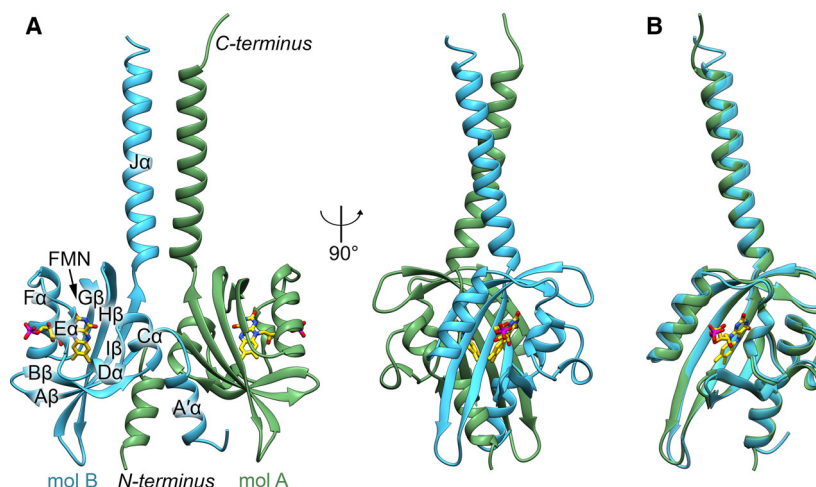


**Table 2.** The interfacial residues of PpSB2-LOV monomers in the dimer within the hydrogen bond distance of  $\leq 3.2$  Å, as observed in the crystal structure.

Secondary structure element	Residue of Chain A	Atom	Distance (Å)	Atom	Residue of Chain B	Secondary structure element
A'α	Asn15	ND2	3.0	OG	Ser98	Hβ
A'α	Asp16	OD1	2.7	NH2	Arg117	Iβ
Hβ	Ser98	OG	3.1	ND2	Asn15	A'α
Iβ	Arg117	NH2	2.8	OD1	Asp16	A'α
Jα	Arg 140	NH2	3.1	OE2	Glu135	Jα

differences in protein sequences where side chains of some residues have different conformational freedoms. For example, L64 and R80 display increase in RMSF in PpSB1-LOV, whereas A74 and A92 show a decrease in RMSF. In addition, residues Q23 (K in PpSB1-LOV), E24 (identical to PpSB1-LOV), and N26 (D in PpSB1-LOV) in PpSB2-LOV display relatively higher dynamics.

In the light state, a covalent adduct is formed between the conserved C53 residue and the chromophore. In order to study the MD of both proteins in the light state, the geometry of the FMN-cysteiny adduct needs to be elucidated first, which will serve as a reference for parameterization, such as bond lengths, bond angles, dihedral angles, and partial charges. To our knowledge, no structure of the FMN-cysteiny adduct is available with atomistic resolution ( $\leq 1$  Å). The FMN-cysteiny adduct has been interpreted from the known crystal structures at nonatomic resolution, which show additional electron density between the cysteine residue and FMN. However, as pointed out by the authors themselves, the FMN-cysteiny adduct is susceptible to radiation damage during the X-ray diffraction experiment and the electron density maps possibly contain a mixture of broken and intact bonds in the crystal [24,25,34]. Therefore, we modeled a structure of FMN-cysteiny adduct based on

lumiflavin(C4a)-isopropyl, which forms a similar covalent adduct (CCDC ID: 1180634) [35]. As described in the methods section, its geometry was optimized with quantum mechanical (QM) calculations using the B3LYP/6 31G\* level of theory.

Structure information for PpSB2-LOV in the light state is not available as the protein did not crystallize under continuous light conditions. We thus modeled it based on the crystal structure of PpSB1-LOV (PDB ID 3SW1) in its light state. During the 200-ns (two times 100 ns) MD simulations, the structure of PpSB1-LOV in the light state remained stable with a constant RMSD fluctuation (Fig. S2). This is not surprising as the crystal structure is expected to be in the lowest energy minimum. In contrast, the model created of PpSB2-LOV light state likely represents only the nearest local energy minimum. During the MD simulation, the structure first explores the conformational space, eventually finding the lowest energy minimum. During the 400-ns (two times 200 ns) simulation, the PpSB2-LOV light-state structure attains equilibrium after 170 ns in each simulation run. This can be seen from significantly lower RMSD fluctuations at later simulation times as compared to that at the beginning (Fig. S2). For this reason, we used 170–200-ns time frame for calculation of RMSF values.



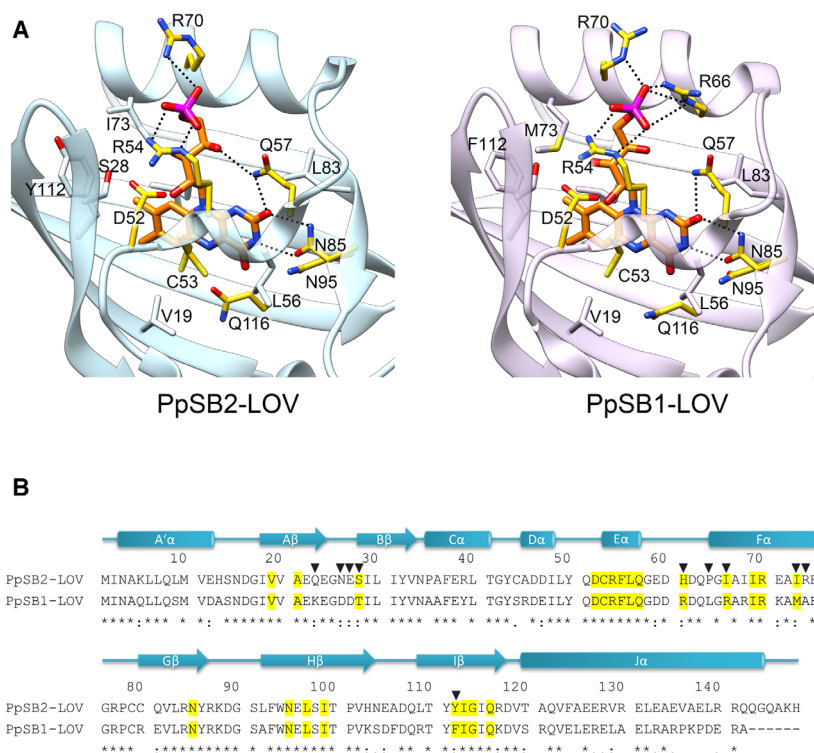


**Fig. 3.** Comparison of the chromophore binding pockets of PpSB2-LOV and PpSB1-LOV in the dark states. (A) PpSB2-LOV (blue) and PpSB1-LOV (PDB ID: 5J3V, [22]) (plum) structures are represented as ribbons and were generated with the UCSF Chimera software [62]. FMN and the interacting residues are shown as stick models colored by element as in Fig. 2. The carbon atoms of the residues within  $\leq 4$  Å distance to FMN are colored in model color. Hydrogen bonds ( $\leq 3.2$  Å) are shown as dotted lines. (B) The sequence alignment of PpSB2-LOV (UniProt-ID: Q88JB0) with PpSB1-LOV (UniProt-ID: Q88E39), generated with the Clustal Omega program [67]. The secondary structure elements for PpSB2-LOV are shown on top, where: arrow— $\beta$ -strand and cylinder— $\alpha$ -helix. The asterisks at the bottom line of the alignment indicate identical residues in a given sequence position, while single and double dots refer to highly and moderately similar residues, respectively. Residues lining the chromophore pocket at cutoff distances  $\leq 4$  Å from FMN in the PpSB2-LOV crystal structure are highlighted in yellow. Substitution mutations described in the text are marked with arrowheads above the sequence.

The RMSF of the core domain residues 17–119 of PpSB2-LOV and PpSB1-LOV was calculated during their MD simulations in the light state (Fig. 4B) (the corresponding residue numbers in Oat Phototropin 1, AsLOV2 are 414–517). The RMSF of main chain atoms (N, C $\alpha$ , C, and O) for most of the structure remained similar between PpSB2-LOV and PpSB1-LOV in the light state. However, higher RMSF values were observed for residues in A $\beta$ -B $\beta$  and H $\beta$ -I $\beta$  loops, the F $\alpha$  helix and the G $\beta$  strand. Considering that there is only minor difference in the side chain RMSF of the F $\alpha$  helix and the G $\beta$  strand residues, this can be interpreted as a concerted motion. Notably, several residues with higher RMSF values in the A $\beta$ -B $\beta$  loop, the E $\alpha$ -F $\alpha$  loop, and the F $\alpha$  helix are located in close proximity to FMN and are part of the chromophore pocket in the crystal structure. In the LOV photocycle, a covalent bond is formed between the photoactive cysteine residue and the C4a atom of the flavin

chromophore upon blue-light illumination, and the FMN N5 atom is protonated [36], with the proton likely originating from the photoactive cysteine or a water molecule. In the dark, the FMN-cysteinyl thiol adduct is thermally broken and the FMNH-N5 atom deprotonated to conclude the photocycle. Compared to PpSB1-LOV, several residues lining the chromophore pocket show higher dynamics in PpSB2-LOV (see inset in upper panel of Fig. 4B), which might be related to increased solvent accessibility to the chromophore.

### PpSB2-LOV shows larger solvent-accessible cavities

Next, we compared the solvent-accessible cavities for PpSB2-LOV and PpSB1-LOV crystal structures by scanning the binding pocket with a standard 1.4 Å probe radius (Fig. 5). The cavity volume essentially

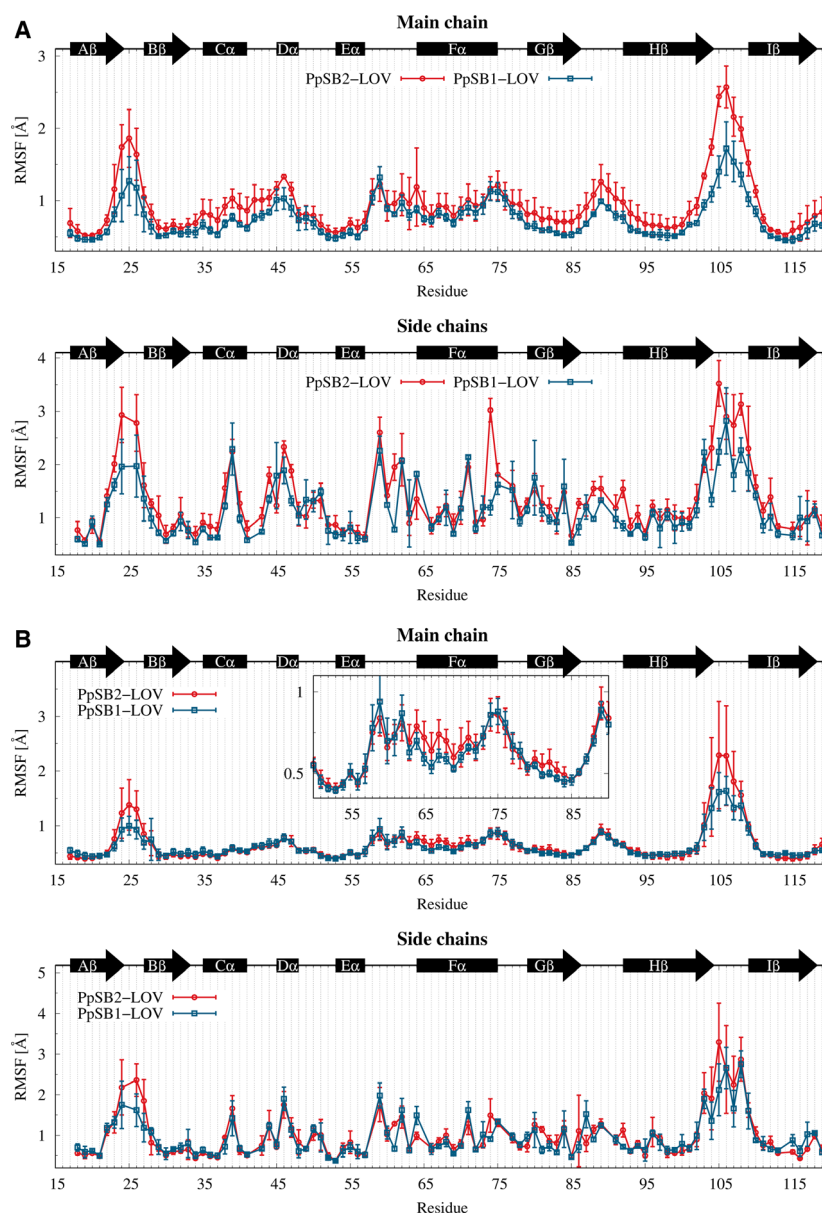


**Fig. 4.** Residue-resolved RMSF from MD simulations of the PpSB2-LOV and PpSB1-LOV. (A) in the dark states and (B) in the light states. The bars indicate the values of two monomers, whereas the points indicate their average. The secondary structure elements of PpSB2-LOV are shown as arrows for strands and rectangles for helices. Secondary structure assignment was done with the DSSP program [65] for the PpSB2-LOV crystal structure.

reflects shape of the chromophore together with its solvent accessibility. The PpSB2-LOV cavity shows protrusions both in the direction of the E $\alpha$ -F $\alpha$  loop and in the direction of the C-terminal end of the F $\alpha$  helix. Extended cavity volume might indicate higher solvent accessibility to FMN in PpSB2-LOV as compared to that in PpSB1-LOV. The rate-limiting step for the thermally driven dark recovery is the deprotonation of the FMN-N5 [30,37]. Previous reports have suggested a water molecule as a proton acceptor for the deprotonation of the FMNH-N5 atom [38,39]. An increased solvent accessibility in PpSB2-LOV may thus enable water to readily enter the chromophore-binding pocket,

promoting the deprotonation rates of the FMN-N5, and accelerate dark recovery, as has been suggested previously for *Avena sativa* LOV2 domain [38].

The extension of the PpSB2-LOV solvent-accessible cavity toward the F $\alpha$  helix and E $\alpha$ -F $\alpha$  loop as well as the slightly different conformation of this loop might be linked to the differences in the amino acid sequence when compared with PpSB1-LOV. For example, both R61 and R66 in PpSB1-LOV are part of an arginine cluster that is unique among available LOV structures and comprises four arginine residues involved in formation of salt bridges with the flavin phosphate moiety [6]. In PpSB2-LOV structure, the corresponding

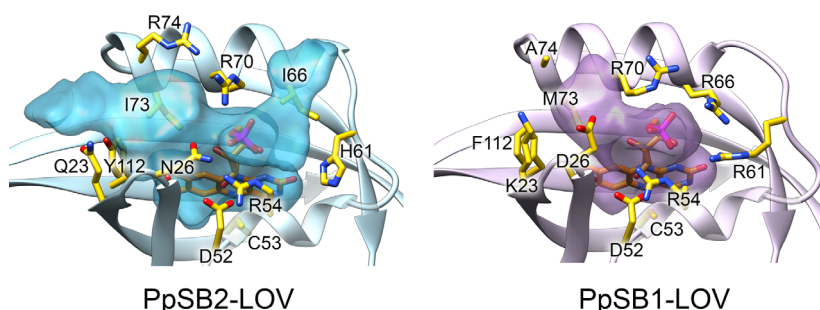


**Fig. 5.** Solvent-accessible cavities of the PpSB2-LOV (blue) and PpSB1-LOV (PDB ID: 5J3W, [22]) (plum) cavities with several interacting residues in the close proximity shown as stick models colored by element as in Fig. 2. The figure shown was generated with the UCSF Chimera software [62].

residues are H61 (charged) and I66 (hydrophobic), where the side chain of H61 is directed away from the phosphate group of FMN. Lower conformational freedom of the side chains and shorter lengths thus do not allow interaction with the phosphate group.

### Substitution mutations in A $\beta$ strand, A $\beta$ -B $\beta$ loop, and F $\alpha$ helix in PpSB2-LOV alter the adduct life time

Comparison of MD simulations performed on PpSB2-LOV and PpSB1-LOV under dark and light conditions indicates higher protein dynamics in PpSB2-LOV. Specifically, residues surrounding the solvent cavity located in A $\beta$  strand, A $\beta$ -B $\beta$  loop, and F $\alpha$  helix (Fig. 4). In addition, the solvent cavity calculations show a larger cavity in PpSB2-LOV (Fig. 5). A pairwise sequence alignment revealed differences in several residues in the region (Fig. 3B). We thus speculated that protein dynamics and solvent accessibility might be responsible for differences in the adduct-state lifetimes in PpSB2-LOV and PpSB1-LOV proteins. To test this hypothesis, we performed stepwise site-directed mutagenesis by mutating PpSB2-LOV residues to the equivalent residues of PpSB1-LOV. In the first step, we chose following single point mutations based on comparative structure analysis, proximity to the chromophore-binding pocket and MD simulations. For comparison, the corresponding residues in the most commonly known LOV2 domain of *A. sativa* (Oat) are listed in Table 3. In A $\beta$  strand and A $\beta$ -B $\beta$  loop: Q23K, N26D, E27D, S28T; in F $\alpha$  helix: P64L, I73M, R74A; and in I $\beta$ : Y112F (Fig. 6, Table 3). Side chain of Y112 is involved in hydrogen bond interactions with Q23 of A $\beta$ -B $\beta$  loop. We therefore rationalized that this position could have an impact on the loop conformation, which in turn would affect the solvent accessibility to the bound chromophore thus changing adduct stability. A previous study has examined adduct-state lifetime of Q23K and E71K mutants in crude cell extract and of H61R and I66R mutants with purified proteins [7]. We measured these mutants with our setup to allow a reliable

comparison. Mutants E27D and I66R showed an increased adduct life time by more than five times, Q23K and H61R by 2.3 and 1.5, respectively, while others had slightly accelerating (S28T, P64L, I73M, R74A) or no effect (N26D) (Table 3). Mutants that result in an adduct-state lifetime that is more than two-fold longer or shorter are referred to as decelerating and accelerating mutants, respectively. For clarity, the accelerating and decelerating mutants in Table 3 are colored green and red, respectively.

To further investigate role of above-mentioned mutations on the adduct-state lifetime, we made double mutants in several combinations such as in A $\beta$  & A $\beta$ -B $\beta$  loop; A $\beta$  & B $\beta$ ; A $\beta$  & F $\alpha$ ; A $\beta$  & I $\beta$ ; B $\beta$  & I $\beta$ ; and F $\alpha$  & I $\beta$  (Table 3). Most mutants show an increase in adduct-state lifetime, with the most pronounced increase (5- to 10-fold) observed in mutants containing the mutations E27D or I66R. In contrast, the presence of mutations S28D and I73M resulted in up to twofold acceleration of the dark recovery. Notably, the point mutations Q23K and H61R lead to a moderate increase in adduct lifetime, but they significantly enhance this effect in combination with the strongly decelerating mutants E27D and I66R (Table 3).

These findings encouraged us to investigate multiple mutants, which are listed in three clusters in Table 3 for the sake of clarity: Cluster 1 consists of mutants that have Q23K and E27D common in all. Two interesting observations here are that firstly, all mutants showed an increase in adduct-state lifetime, and secondly, the slowing effect of mutations on the dark recovery process is considerably additive. For example, Q23K N26D E27D S28T showed a  $\sim 7$ -fold increase in the adduct-state lifetime, which was further enhanced to  $\sim 30$ -fold when combined with I66R (Table 3, Cluster 1). Addition of H61R to the latter further enhanced the deceleration effect to  $\sim 58$ -fold.

As a second example, the single mutants H61R and I66R show increase in adduct lifetimes by 1.5- and 5.5-fold. In combination, the double mutant H61R/I66R led to an 11-fold increase in the adduct-state



**Table 3.** Dark recovery time constants of PpSB2-LOV substitution mutants, based on the PpSB1-LOV protein. All measurements were performed at 20 °C. Color code for amino acids: red: decelerating; green accelerating, black neutral. Residues E27D and I66R significantly affect the adduct lifetime and are highlighted in bold. \*The corresponding residues in the most commonly known LOV2 domain of *Avena sativa* (Oat) are listed.

PpSB2-LOV mutant (based on PpSB1-LOV protein sequence)	<i>AsLOV2*</i>	Dark recovery $\tau_{\text{rec}}$ (min)	x-fold increase of adduct life time	Secondary structure location
PpSB2-LOV (wild-type)		3.5	1.0	-
<b>I. Single Mutants (n = 1)</b>				
<b>Q23K</b>	(P420)	7.9	2.3	A $\beta$
N26D	(P423)	3.5	1.0	A $\beta$ -B $\beta$ loop
<b>E27D</b>	(D424)	19.0	5.6	A $\beta$ -B $\beta$ loop
<b>S28T</b>	(N425)	1.7	0.5	B $\beta$
H61R	(T458)	5.2	1.5	Ea-Fa loop
P64L	(A461)	2.2	0.6	Ea-Fa loop
<b>I66R</b>	(V463)	18.7	5.5	Fa
<b>I73M</b>	(I470)	1.3	0.4	Fa
R74A	(D471)	2.2	0.6	Fa
Y112F	(F509)	4.3	1.3	I $\beta$
<b>II. Double Mutants (n = 2)</b>				
<b>Q23K N26D</b>		7.9	2.3	A $\beta$ and A $\beta$ -B $\beta$ loop
<b>Q23K E27D</b>		35.3	10.4	A $\beta$ and A $\beta$ -B $\beta$ loop
<b>N26D E27D</b>		19.0	5.6	A $\beta$ -B $\beta$ loop
<b>Q23K S28T</b>		5.9	1.7	A $\beta$ and B $\beta$
<b>Q23K I73M</b>		3.0	0.9	A $\beta$ and Fa
<b>Q23K I66R</b>		35.5	10.5	A $\beta$ and Fa
<b>Q23K Y112F</b>		9.4	2.8	A $\beta$ and I $\beta$
<b>S28T I73M</b>		1.6	0.5	B $\beta$ and Fa
<b>S28T Y112F</b>		2.7	0.8	B $\beta$ and I $\beta$
<b>H61R I66R</b>		37.6	11.1	Ea-Fa loop and Fa
<b>I73M R74A</b>		1.7	0.5	Fa
<b>I73M Y112F</b>		1.7	0.5	Fa and I $\beta$
<b>III. Multiple mutants (n <math>\geq</math> 3)</b>				
<b>Cluster 1</b>				
<b>Q23K N26D E27D</b>		31.5	9.3	A $\beta$ and A $\beta$ -B $\beta$ loop
<b>Q23K N26D E27D S28T</b>		24.5	7.2	A $\beta$ , A $\beta$ -B $\beta$ loop, B $\beta$
<b>Q23K N26D E27D S28T I66R</b>		101.4	29.9	A $\beta$ , B $\beta$ , A $\beta$ -B $\beta$ loop and Fa
<b>Q23K N26D E27D S28T H61R I66R</b>		198.4	58.4	A $\beta$ , B $\beta$ , loops A $\beta$ -B $\beta$ , Ea-Fa and Fa
<b>Q23K E27D H61R I66R</b>		137.7	40.6	A $\beta$ , loops A $\beta$ -B $\beta$ , Ea-Fa and Fa
<b>Q23K H61R I66R</b>		67.9	20.0	A $\beta$ , Ea-Fa loop and Fa
<b>Cluster 2</b>				
<b>E71K I73M R74A</b>		1.9	0.6	Fa
<b>I66R I73M R74A</b>		56.4	16.6	Fa
<b>I66R E71K I73M R74A</b>		69.4	20.4	Fa
<b>P64L E71K I73M R74A</b>		1.8	0.5	Ea-Fa loop and Fa
<b>P64L I66R E71K I73M R74A</b>		57.6	17.0	Ea-Fa loop and Fa
<b>H61R P64L I66R E71K I73M R74A</b>		131.2	38.6	Ea-Fa loop and Fa
<b>Cluster 3</b>				
<b>Q23K S28T I73M</b>		1.4	0.4	A $\beta$ , B $\beta$ and Fa
<b>Q23K S28T Y112F</b>		6.1	1.8	A $\beta$ , B $\beta$ and I $\beta$
<b>Q23K I73M Y112F</b>		2.9	0.8	A $\beta$ , Fa and I $\beta$
<b>Q23K S28T I73M Y112F</b>		1.5	0.5	A $\beta$ , B $\beta$ , Fa and I $\beta$
<b>Q23K N26D E27D S28T I73M Y112F</b>		5.9	1.7	A $\beta$ , B $\beta$ , A $\beta$ -B $\beta$ loop, Fa and I $\beta$
<b>S28T I73M Y112F</b>		1.1	0.3	B $\beta$ , Fa and I $\beta$
<b>S28T P64L I73M Y112F</b>		0.8	0.2	B $\beta$ , Fa and I $\beta$
<b>S28T I73M R74A Y112F</b>		1.3	0.4	B $\beta$ , Ea-Fa loop, Fa and I $\beta$

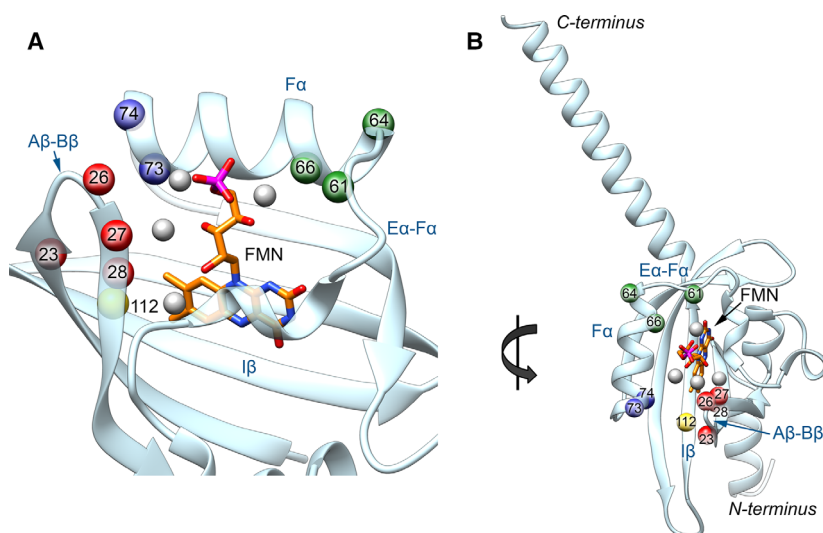


**Fig. 6.** Mutation sites in A $\beta$ , A $\beta$ -B $\beta$  loop, and F $\alpha$  helix in PpSB2-LOV (A) Ribbon representation of the PpSB2-LOV core domain with the orientation as in Fig. 3A. Residues mutated in this study are shown as filled circles. A $\beta$  and A $\beta$ -B $\beta$  loop—Red, E $\alpha$ -F $\alpha$  loop and N terminus of F $\alpha$  helix—Green, C terminus of F $\alpha$  helix—Blue, I $\beta$ —Yellow. Conserved water molecules in the chromophore pocket are shown as filled gray circles (B) Complete protein chain showing the mutation sites. Compared to panel A, this view is rotated by roughly 90° along the y-axis. Representations in both the panels were generated with the UCSF Chimera software [62].

lifetime. As a triple mutant Q23K H61R I66R incorporating the mutation Q23K, the same effect is increased 20-fold, and again to 40-fold in the quadruple mutant Q23K E27D H61R I66R.

In cluster 2, we have listed the mutants primarily located on F $\alpha$  helix and the preceding loop E $\alpha$ -F $\alpha$ . Several residues in the region are involved in the hydrogen-bonding network with the FMN chromophore. A combination of F $\alpha$  mutations (I66R E71K I73M R74A) resulted in a 20-fold slower dark recovery. Excluding I66R from the same mutant, however, produces an opposite result where a moderate twofold acceleration was observed in the triple mutant E71K I73M R74A. The acceleration effect is likely due to the presence of mutation I73M, which shows 2.5-fold acceleration when mutated alone (Table 3). The stepwise incorporation of P64L, I66R, and H61R into the triple mutant E71K I73M R74A yields 4er, 5er, and 6er mutants that show a slight acceleration, a 17-fold deceleration, and a 39-fold deceleration, respectively. Cluster 2 again demonstrates that I66R mutation has a significant effect on stabilization of the adduct and hence in slowing down of the dark recovery process.

Multiple mutants incorporating the accelerating mutations S28T and/or I73M are listed in Cluster 3. Mostly, the mutants show an acceleration of dark recovery kinetics with up to fivefold increase in the triple and quadruple mutants that consist of both, S28T and I73M. We show above that E27D is a strong decelerating mutation. The sextuple mutant, which is a combination of a deceleration mutant Q23K N26D E27D (ninefold slower dark recovery) and the acceleration mutant S28T I73M Y112F (fivefold faster dark recovery), displays only a 1.7-fold increase in the adduct lifetime. The presence of the accelerating mutations S28T

and I73M is thus sufficient to diminish the deceleration effect of Q23K and E27D mutations.

#### Hydrogen bonding and hydrophobic interactions on the periphery of chromophore pocket influence adduct-state lifetime

While the direct impact of the I66R and H61R mutations was expected and can be rationalized in terms of solvent-access (see above) and/or by constraining the orientation of the phosphate moiety and possibly of the whole FMN molecule in the light state [6], the impact of the other accelerating and decelerating mutations is more difficult to discern.

In order to get more insight into specific interaction of mutated residues, we have analyzed MD simulation data of PpSB2-LOV and PpSB1-LOV. Specifically, we looked for hydrogen bonding and salt-bridge formations (Table S1).

Residue E27/D27 participates in hydrogen bonding/salt-bridge formation in both the PpSB2-LOV and PpSB1-LOV proteins mainly with R54. The latter coordinates tightly with the phosphate group of the FMN chromophore. The side chain of D27 in PpSB1-LOV is, however, shorter than that of E27 and one can speculate that the A $\beta$ -B $\beta$  loop bends closer onto the chromophore, hindering the solvent access from this side of the pocket.

D26 in PpSB1-LOV and N26 in PpSB2-LOV, both form hydrogen bonds to R70 and N26 additionally to R54. Both these arginine residues coordinate phosphate group of FMN and have been predicted to play a significant role in adduct stabilization [6].

For the residues 23 and 28, we could not find strong change in hydrogen-bonding partner during course of

simulation, except that Q23 in PpSB2-LOV in comparison with K23 had more diverse interaction partners including the side chain of Y112. Overall, it suggests that increased hydrophobicity of the side chain may play a role in controlling the solvent accessibility to the chromophore. This might be related to the slower dark recovery of PpSB1-LOV where Y112 lining the chromophore pocket is replaced by F112 (Fig. 3). Another residue lining the pocket, M73 in PpSB1-LOV has a longer side chain and can interact more effectively with the F112 via hydrophobic interactions than I73 in PpSB2-LOV.

For E71K and R74A mutation, it is not evident from our data how they can contribute to the adduct stabilization or destabilization. The changes we here observed were in their interaction partners, where K71 in PpSB1-LOV interacts with E75 both in crystal structure and in MD simulation, whereas E71 in PpSB2-LOV shows interactions during MD simulation with R74 and R77.

## Discussion

In bacteria, fungi, protists, and land plants, the so-called short LOV protein family, lacking fused effector domains, represents the third largest LOV photoreceptor family [4]. The PpSB1-LOV/PpSB2-LOV short LOV photoreceptors of *P. putida* KT2440 are among the most well-studied short LOV photoreceptors [6,7,11,17,22,23,40]. PpSB1-LOV is a very slow-cycling short LOV protein with an adduct-state lifetime  $\tau_{\text{REC}} = 2467$  min at 20 °C. PpSB2-LOV from the same organism, in contrast, shows a relatively fast dark recovery  $\tau_{\text{REC}}$  of  $\sim 3.5$  min at 20 °C. Both the proteins share 67% sequence identity. The crystal structure of PpSB2-LOV in the dark state presented here shows that the overall structure is similar among the three-known short LOV protein structures (PpSB1, PpSB2, and W619\_1) from *P. putida* [6,17,22]. A significantly higher resolution of 1.9 Å in PpSB2-LOV provides additional insight into molecular details, including the presence of structured water molecules in the solvent channel, which could not be observed previously in the other three structures due to moderate resolution ( $\geq 2.5$  Å). Furthermore, almost all residues in the J $\alpha$  helix (residues 120–148) are resolved which is 12 residues longer than that of PpSB1-LOV, and is the longest C-terminal J $\alpha$  helix among the known *Pseudomonas* LOV protein structures. In most LOV proteins, the J $\alpha$  helix is the connecting link for signal relay from the sensor to the effector domain. Among the  $\gamma$ -proteobacterial short LOV proteins, the C-terminal J $\alpha$ -helix is variable in both sequence and length [40]. We previously proposed

signaling mechanism for the *Pseudomonas* LOV protein dimers, where rotation of two protein chains relative to each other causes large movements in the C-terminal J $\alpha$  helices, relaying the light-activated signal from the sensor to the associated effector domains [22]. This mechanism was based on the comparative analysis of dark and fully light-adapted state crystal structures of PpSB1-LOV. PpSB2-LOV did not crystallize under light conditions, which is most likely due to a relatively fast dark recovery that makes it difficult to maintain a steady-state population of the adduct under illumination. Crystallization of LOV proteins alone in fully light-adapted state has been successful only in selected cases that show very slow dark recovery [6,25]. We obtained the light-state model for PpSB2-LOV from MD simulations based on the PpSB1-LOV light-state structure, where the model is allowed to explore the conformational space and arrive at a more plausible structure than a homology model that is mainly guided by the template. Very low RMSD changes over time (Fig. S2) for the constructed light-state dimer suggest highly similar structural conformations in the light state of both, PpSB2-LOV and PpSB1-LOV proteins. In addition, superposition of the PpSB2-LOV structural model for the dark and the light states reveals global conformational changes described previously in PpSB1-LOV and corroborate signaling mechanism similar to the PpSB1-LOV protein (Fig. 7). PpSB2-LOV is thus the second example, after PpSB1-LOV, to corroborate this signaling mechanism, which might also be transferred to other structurally conserved short LOV proteins from different *Pseudomonas* species.

The structure alone, however, is not sufficient to explain the vast differences in adduct-state lifetimes among this class of structurally conserved short LOV proteins. MD simulations presented in this work reveal higher dynamics in the A $\beta$  strand, A $\beta$ -B $\beta$  loop, and F $\alpha$  helix in PpSB2-LOV (Fig. 4). By combining MD simulation results with sequence and structural homology to PpSB1-LOV, we generated substitution mutants in PpSB2-LOV to identify the residues responsible for the differences in adduct-state lifetimes between the two proteins (Table 3). Previous mutagenesis studies have demonstrated that a subtle change in the residue type can lead to considerable alterations in the adduct lifetime [29,38,41,42]. In PpSB2-LOV, residue positions 27 (424 in *AsLOV2*) and 66 (V463 in *AsLOV2*) play a central role while 23 (420 in *AsLOV2*) and 61 (458 in *AsLOV2*) likely work cooperatively in stabilization of the adduct and hence slowdown of the dark recovery. In contrast, positions 28 (425 in *AsLOV2*) and 74 (471 in *AsLOV2*) have an opposite effect, increasing the rate of dark recovery. All the residues mutated in this

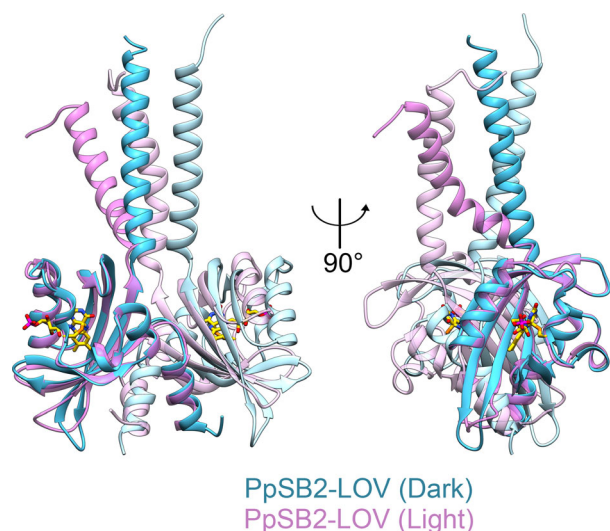


**Fig. 7.** Structural differences between the dark- and the light-state dimers of PpSB2-LOV. Ribbon representations showing superposition of PpSB2-LOV dark state (blue) and light state (pink), generated with the UCSF Chimera software [62]. The structure alignment was done for the LOV core domains of single protein chains (shown left). A  $\sim 29^\circ$  rotation and translation of the core domain in the counterpart (chain shown on right) are required to superpose the two dimers on each other. The FMN molecules are shown as stick models, and the twofold axis runs from top to bottom.

study are in the vicinity of the chromophore pocket (Fig. 6). Interestingly, several of the residues interact with the conserved water molecules bound to the chromophore (Fig. 6). We analyzed crystal structures of the LOV domains listed in PDB database with a resolution of 2.0 Å and higher for the chromophore-bound water molecules and observed that both, the water molecules as well as the FMN–water and FAD–water interactions are well conserved (Tables S2,S3). Notably, the solvent-accessible cavities calculated for PpSB2-LOV are significantly large compared with that in PpSB1-LOV (Fig. 5). The cavity is extended toward the A $\beta$ –B $\beta$  loop, E $\alpha$ –F $\alpha$  loop, and F $\alpha$  helix, which outlines the solvent channel to the chromophore. The MD simulations suggest increased flexibility in the residues located in the aforementioned secondary structure elements implying their role in adduct stabilization or destabilization by controlling the solvent/base accessibility. Residues in close proximity to the solvent channel have been previously reported to attenuate the adduct decay rates by altering the stability of the N5 protonation state and hydrogen bonding to the active site flavin [29,30,43].

The dark-state structure of PpSB2-LOV shows two conformations of the active cysteine (C53). The same has been observed in several other LOV structures in

the dark state where the first conformation positions the active cysteine above the C4a position and is favorable for adduct formation whereas the second conformation orients away [31,33] and was suggested to destabilize the light-state adduct [29,30]. Mutations altering the steric factors that favor the first conformation will thus have a stabilizing effect and result in longer adduct lifetime. Even though none of the residues mutated in the current study shows direct H-bonding interactions with the isoalloxazine ring of the bound FMN, they form the border of the solvent channel. An increased density of electrons as a result of mutations such as increase in hydrogen bonding near the pyrimidine ring of flavin can stabilize the light-state adduct [44,45]. And in contrast, factors favoring deprotonation of the N5 position of the isoalloxazine ring contribute to a faster decay [30,44,45]. Many of the mutated residues such as S28, H61, I66, and I73 are hydrogen bonded to the conserved water molecules in the chromophore pocket. Mutation of these residues is expected to affect the H-bond network, steric contacts as well the electron distribution within the flavin system. In PpSB1-LOV, four arginine residues R54, R61, R66, and R70 form a unique cluster of salt bridges with the FMN phosphate moiety. Current work and previous mutational studies demonstrate an important role of the side chain interactions such as H-bonds or salt bridges with the FMN phosphate group in controlling the adduct lifetime [6,7,46]. I66R mutant in PpSB2-LOV results in more than five-fold increase in the adduct lifetime. The reverse mutation in PpSB1-LOV had even more dramatic effect where the adduct lifetime decreased by a factor of more than 100 in PpSB1-LOV mutant R66I [7].

In conclusion, LOV domains have proven useful in the development of optogenetic tools where the photoresponsive LOV domain forms the input module to activate/regulate diverse signal transduction domains. In Table 3, we report several PpSB2-LOV mutants with the dark recovery time ranging from seconds to hours, providing a broad selection that can be utilized for the generation of optogenetic tools with very specific on/off kinetic requirements. Considering the similarities and structural conservation between the short LOV proteins from *Pseudomonas* family [6,17,22,40], the photocycle tuning strategies from this study can likely be extended to other LOV proteins. An important issue that we cannot address with our study is the impact of the presented mutations on the signal relay process, since no functional read-out assay is available to probe the functionality of the presented variants of PpSB2-LOV. Please note, however, that we have only introduced interchanging mutations between two



homologous proteins; that is, amino acids were interchanged between the slow reverting PpSB2-LOV and the fast reverting PpSB1-LOV. For example, PpSB2-LOV harbored a Gln at position 23, while PpSB1-LOV contained a Lys at the corresponding position. Consequently, we introduced the Q23K mutation in PpSB2-LOV. We are thus only exchanging amino acids between two natural photoreceptors, which should render the mutations structurally and presumably also functionally more benign than, for example, mutations that are not found in nature. This hypothesis is partially corroborated in a recent study by Hart *et al.*, which performed targeted mutagenesis on *Arabidopsis* phot1 and phot2 to modify their photocycle to enhance their responsiveness and to promote plant growth [46]. They show that tuning the phototropin photocycle can reduce or extend the duration of photoreceptor activation *in planta*. Plants engineered to have a slow-photocycling variant of phot1 or phot2 displayed increased biomass production under low-light conditions as a consequence of their improved sensitivity, and plants with fast-cycling variants exhibit reduced phototropin's sensitivity for chloroplast accumulation movement. One of the very effective mutants in extending the adduct lifetime reported by the authors is in fact V525R, which is equivalent to I66R in PpSB2-LOV. The study highlights that one of the mutations, which had the most pronounced impact in the present study, does not negatively influence the signal relay process in full-length phototropin. Nevertheless, further work is needed to probe the functional impact of the here presented mutations on the signal relay in the *Pseudomonas* short LOV family. In fact, the two short LOV photoreceptors, PpSB1-LOV and PpSB2-LOV, were recently implicated in light-dependent gene expression process in *P. putida* KT2440 [11]. The use of knockout strains in combination with gene expression studies as presented by Sumi *et al.* [11] would open up the possibility to probe the functional impact of PpSB1-LOV/PpSB2-LOV mutations, which, however, exceeds the scope of the present study. Both, the results presented in our study and the previous results by Hart *et al.* emphasize the importance of a mechanistic understanding of photocycle tuning in LOV proteins, especially in the context of their potential applications.

## Materials and methods

### Protein expression

The gene encoding PpSB2-LOV (Swiss Prot: Q88JB0) was cloned as described previously [7]. In brief, a construct of

PpSB2-LOV possessing N-terminal hexahistidine tag (tag sequence: MGSSHHHHHSSGLVPRGSH) was expressed in *E. coli* BL21 (DE3). Autoinduction (AI) media was prepared with Terrific Broth medium (X972; Carl-Roth, Karlsruhe, Germany) and supplemented with 50  $\mu\text{M}$  riboflavin (A6279; AppliChem GmbH, Darmstadt, Germany), 50  $\mu\text{g}\cdot\text{mL}^{-1}$  kanamycin and for induction, 0.5  $\text{g}\cdot\text{L}^{-1}$  glucose, and 2  $\text{g}\cdot\text{L}^{-1}$  lactose. Overexpression was carried out in 250 mL AI media cultures for 3 h at 37 °C. Afterward, the incubation temperature was changed to 30 °C and the cells were incubated for 24 h with constant agitation at 110 r.p.m.

### Protein purification

The cell pellet (5 g cells, wet weight) was dissolved in 30 mL of lysis buffer [50 mM  $\text{NaH}_2\text{PO}_4/\text{Na}_2\text{HPO}_4$ , 300 mM NaCl, and 10 mM imidazole (pH 8.0)]. The cells were then lysed by passing the cell suspension through a Microfluidizer three times at a constant pressure of 2000 bar. The soluble fraction was separated from the pellet by centrifugation at 50 000 *g* for 30 min at 4 °C. The supernatant was purified by IMAC using a Superflow Ni-NTA resin (QIAGEN; Hilden, Germany) with the gravity flow protocol. The standard column volume (CV) of the Ni-NTA resin was 5 mL. The lysate was applied to the resin and washed with 10 CV of lysis buffer and 5 CV of wash buffer [50 mM  $\text{NaH}_2\text{PO}_4/\text{Na}_2\text{HPO}_4$ , 300 mM of NaCl, and 40 mM imidazole (pH 8.0)]. Elution was performed with 5 CV of elution buffer [50 mM  $\text{NaH}_2\text{PO}_4/\text{Na}_2\text{HPO}_4$ , 300 mM NaCl, and 250 mM imidazole (pH 8.0)]. The purity of the eluted fractions was evaluated by SDS/PAGE.

The pure protein fractions were pooled, and the elution buffer was exchanged to the storage buffer [10 mM Tris pH 8.0, 10 mM NaCl], using ÄKTA pure FPLC system (GE Healthcare, Buckinghamshire, UK) with an HiPrep 26/10 Desalting column as per standard protocol. The protein fractions were pooled, supplemented with 3 mM Tris(2-carboxyethyl)phosphine (TCEP), and concentrated by ultrafiltration using Vivaspin centrifugal concentrator units (molecular mass cutoff: 10 kDa) (Sigma-Aldrich; St. Louis, MO, USA). All steps were performed at 4 °C, with only the buffer exchange procedure done at room temperature (20 °C).

### Chromophore content and loading

In order to achieve higher chromophore loading *in vitro*, FMN was added to the protein sample to the final concentration of 10 mM and subsequently incubated overnight in the dark at 4 °C. Unbound chromophore was removed by size-exclusion chromatography using a HiLoad 26/600 Superdex 200 pg column (GE Healthcare) on an ÄKTA pure FPLC system at room temperature. Fractions containing purified protein were pooled, supplemented with 3 mM TCEP, and concentrated as described above.

Chromophore content and quantification of PpSB2-LOV was done with HPLC (Agilent Technologies, Inc., Santa Clara, CA, USA) according to protocol described previously [47]. The total chromophore loading was quantified using protocol described before [17].

### Spectroscopic techniques

UV/Vis Spectroscopy measurements were carried out with a Shimadzu UV-1800 spectrometer (Shimadzu, Kyoto, Japan). All measurements were done at  $20 \pm 2$  °C in 1.5- or 1-mL quartz cuvette with 1 cm light path and in buffer with 10 mM sodium phosphate buffer at pH 8.0, supplemented with 10 mM NaCl. For generation of the light state, the sample was illuminated for at least 30 s using a blue-light ( $\lambda_{\text{max}} = 450$  nm) emitting LED with a radiant power of 50 mW (Luxeon Lumileds; Phillips, Aachen, Germany). Dark recovery kinetics were measured from the illuminated sample using the protocol described previously [7]. After illumination, the absorbance recovery at 475 nm was recorded as a function of time. Time of measurement varied depending on the dark recovery lifetime ( $\tau_{\text{Rec}}$ ) of the respective mutant. The absorbance data were plotted against time with the Gnuplot program and fitted using monoexponential decay function using following equation:

$$\text{Abs} = a_0 + A e^{-\frac{t}{\tau_{\text{Rec}}}}$$

where  $t$  is the time since illumination, Abs—measured absorbance at 475 nm,  $\tau_{\text{Rec}}$ —is the time constant referred to as the adduct lifetime. All measurements were done in triplicate.

### Single crystal microspectrometry

UV-Vis absorbance spectra in the wavelength range 250–700 nm were recorded using an microspectrometer at ID29S at ESRF (Grenoble, France) [48]. Fluorescence spectra were measured by excitation with a blue-light laser (440 nm, 15 mW, cw mode) of cryocooled crystals at 100 K. Same crystals were annealed to room temperature and illuminated for 10 s with the blue-light laser and subsequently frozen to 100 K prior to measurement of UV-Vis spectra.

### Protein crystallization

The purified protein was concentrated to 8 mg·mL<sup>-1</sup> and crystallized by vapor-diffusion method in 96-well sitting drop plates. Crystals were grown under dark conditions in 1.8  $\mu$ L drops (0.9  $\mu$ L purified protein plus 0.9  $\mu$ L reservoir solution) against 70  $\mu$ L of 100 mM sodium acetate (pH 4.9–5.3), 22–26% (w/v) polyethylene glycol 200, and 3–7% (w/v) polyethylene glycol 3350 at 19 or 14 °C. Typically, clusters of needle crystals appeared within a week.

### Data collection and structure determination

Single crystals of PpSB2-LOV were mounted in loops under dim red light and flash frozen with gaseous nitrogen at temperature 100 K. Native data were recorded at the microfocus beamline ID23-2 at ESRF (Grenoble, France) [49] tuned to a wavelength of 0.8726 Å on the PILATUS3 X 2M detector from Dectris Ltd (Baden, Switzerland) at 100 K. Data collection strategy was based on calculations using the program BEST which accounts for radiation damage and symmetry [50]. Collected data had significant reflections up to 1.93 Å resolution and was processed using the xds software [51].

Space group of PpSB2-LOV crystals was determined to be P2<sub>1</sub> with the Pointless program (part of CCP4 software package [52]). The initial phases were obtained by molecular replacement using MOLREP program (CCP4 package) with a single native dataset. The search model was created from the crystal structure of the homologous protein PpSB1-LOV (PDB ID: 3SW1). Analysis of Matthews coefficients [53] suggested two molecules per asymmetric unit, with Matthews coefficient of 2.22 Å<sup>3</sup>·Da<sup>-1</sup> and a solvent content of 44.6%.

The model was further improved with several cycles of refinement using the PHENIX package [54] and manual rebuilding using the COOT program [55]. Data collection and refinement statistics are listed in Table 1.

### Molecular dynamic simulations

The initial models selected for the MD simulation were following: the dimer structure (Chains B and D) of PpSB1-LOV in the dark state (PDB ID: 5J3W), the dimer structure of PpSB1-LOV in the light state (PDB ID: 3SW1), and the dimer structure of PpSB2-LOV in the dark state (current work). Water, ions, and ligands except FMN were removed from the protein crystal structures. Structure information on PpSB2-LOV in the light state is still missing. Due to high similarity of their structure and sequence, the homology model of PpSB2-LOV in the light state was thus created as following. Each chain of PpSB2-LOV crystal structure was divided into three parts: N-terminal (residues 1–16), core domain (residues 17–119), and C-terminal (residues 120–148). Each part was superposed on the corresponding part of PpSB1-LOV light-state structure. Conformations of identical residues were preserved as seen in PpSB1-LOV, whereas in the case of sequence differences, conformations of residues from the superposed PpSB2-LOV structure were used as guidance. The C-terminal residues 135–148 were not changed as this part is disordered in the PpSB1-LOV crystal structure (residues 120–134). Notably, these terminal residues at the extreme end do not participate in the dimer interface and are solvent exposed (Fig. S1).

Next, we created a model of FMN-cysteinyl adduct based on previously determined crystal structure of

lumiflavin(C4a)-isopropyl that has a covalent adduct similar to FMN-cysteiny adduct (CCDC ID: 1180634) [35]. The FMN with adduct to cysteine residue capped by two alanine residues was modeled, and then, its geometry was optimized with QM calculations using the B3LYP/6 31G\* level of theory implemented in GAMESS program. In previous studies, the bond length of the FMN-cysteiny adduct was assumed to be  $\sim 1.82$  Å, as it is in the C-S bond present in cysteine [56]. However, geometry optimization led to the bond length of 1.96 Å due to the fact that the C4a atom of the FMN-cysteiny is  $sp^3$ -hybridized.

The initial crystal structures and the initial model of PpSB2-LOV in the light state were protonated and parameterized by the pdb2gm program as implemented in the GROMACS 5.1 software (www.gromacs.org) using the AMBER-99SB-ILDN force field [57]. The approach has been tried and reported to show very good agreement with the experimental NMR data [57,58].

The topology for the QM-optimized geometries of FMN-cysteiny and FMN together with the QM-derived partial charges was created with the ACPYPE script [59]. The models were solvated in a periodic box (with  $\geq 12$  Å distance from any protein atom to the edge of the box) with TIP3P water molecules, and neutralized at a 150 mM NaCl concentration. The systems were energy-minimized with the steepest descent method, and followed by the conjugated-gradient method, and afterward equilibrated at temperature of 298 K and 1 bar pressure. Cutoff for the electrostatic interaction with Particle Mesh Ewald algorithm [60] was 10 Å and that for the short-range van der Waals interactions was also 10 Å. The simulation time step was 2 fs, and the trajectories were saved every 10 ps. The dark-state simulations were run two times for 50 ns. The light-state simulations were run two times 100 ns for PpSB1-LOV and two times 200 ns for PpSB2-LOV.

The RMSD fluctuation after 170 ns of MD simulation time became small which indicates that the model of PpSB2-LOV in the light state was in apparent equilibrium. The structure was subsequently energy-minimized, first with steepest descent method followed by the conjugated gradient to yield the final model of PpSB2-LOV in the light state. The root-mean-square fluctuation (RMSF) calculation for the simulation of PpSB2-LOV in the light state was derived from 170 to 200 ns trajectory and that for PpSB1-LOV from 70 to 100 ns trajectory. The RMSF calculation for the dark-state simulations was derived from the whole 50 ns trajectory.

Hydrogen bond analysis was performed with help of the VMD software package [61].

## Graphical representation

Unless otherwise indicated, figures were generated with UCSF Chimera software [62], Molscript [63] and Raster3D [64] using secondary structure assignments as given by the

DSSP program [65]. UV-Vis spectra were plotted with the Gnuplot program [66].

## Acknowledgements

This work was supported by grants from the Federal Ministry of Education and Research (Project OptoSys, FKZ 031A16).

The X-ray diffraction experiments were performed on the beamlines ID23-1, ID23-2 at the ESRF (Grenoble, France). We are grateful to local contact persons at the ESRF for providing help in using beamline. Additionally, we are thankful for support on ID29S beamline for microspectrometry measurements, especially Dr. David von Stetten.

## Conflict of interest

The authors declare no conflict of interest.

## Data Accessibility

Atomic coordinates and structure factors for PpSB2-LOV were deposited in the Protein Data Bank (<http://www.rcsb.org>) under PDB ID 7A6P.

## Author contributions

VA, JG, and RBS conceived and designed the structural studies, MD simulations, and the dark recovery kinetics. VA performed expression, purification, crystallization, production of mutants, MD simulations, and the dark recovery kinetic measurements. VA and JG collected X-ray data and performed structural analysis. VA, JG, UK, KEJ, DW, and RBS analyzed and interpreted the data. RBS, VA, and UK wrote the manuscript with contributions from all co-authors.

## Peer Review

The peer review history for this article is available at <https://publons.com/publon/10.1111/febs.15785>.

## References

- Möglich A, Yang X, Ayers RA & Moffat K (2010) Structure and function of plant photoreceptors. *Annu Rev Plant Biol* **61**, 21–47.
- Herrou J & Crosson S (2011) Function, structure and mechanism of bacterial photosensory LOV proteins. *Nat Rev Microbiol* **9**, 713–723.
- Endres S, Granzin J, Circolone F, Stadler A, Krauss U, Drepper T, Svensson V, Knieps-Grunhagen E, Wirtz A,

- Cousin A *et al.* (2015) Structure and function of a short LOV protein from the marine phototrophic bacterium *Dinoroseobacter shibae*. *Bmc Microbiol* **15**, 30.
- 4 Glantz ST, Carpenter EJ, Melkonian M, Gardner KH, Boyden ES, Wong GK & Chow BY (2016) Functional and topological diversity of LOV domain photoreceptors. *Proc Natl Acad Sci USA* **113**, E1442–E1451.
  - 5 Zoltowski BD, Schwerdtfeger C, Widom J, Loros JJ, Bilwes AM, Dunlap JC & Crane BR (2007) Conformational switching in the fungal light sensor Vivid. *Science* **316**, 1054–1057.
  - 6 Circolone F, Granzin J, Jentzsch K, Drepper T, Jaeger KE, Willbold D, Krauss U & Batra-Safferling R (2012) Structural basis for the slow dark recovery of a full-length LOV protein from *Pseudomonas putida*. *J Mol Biol* **417**, 362–374.
  - 7 Jentzsch K, Wirtz A, Circolone F, Drepper T, Losi A, Gärtner W, Jaeger KE & Krauss U (2009) Mutual exchange of kinetic properties by extended mutagenesis in two short LOV domain proteins from *Pseudomonas putida*. *Biochemistry* **48**, 10321–10333.
  - 8 Metz S, Jager A & Klug G (2012) Role of a short light- and singlet oxygen-dependent gene regulation in *Rhodobacter sphaeroides*. *Microbiology* **158**, 368–379.
  - 9 Schwerdtfeger C & Linden H (2003) VIVID is a flavoprotein and serves as a fungal blue light photoreceptor for photoadaptation. *EMBO J* **22**, 4846–4855.
  - 10 Hendrischk AK, Moldt J, Fruhwirth SW & Klug G (2009) Characterization of an unusual LOV domain protein in the alpha-proteobacterium *Rhodobacter sphaeroides*. *Photochem Photobiol* **85**, 1254–1259.
  - 11 Sumi S, Mutaguchi N, Ebuchi T, Tsuchida H, Yamamoto T, Suzuki M, Natsuka C, Shiratori-Takano H, Shintani M, Nojiri H *et al.* (2020) Light-response of *Pseudomonas putida* KT2440 mediated by class II LitR, a photosensor homolog. *J Bacteriol* e00146-20.
  - 12 Kottke T, Heberle J, Hehn D, Dick B & Hegemann P (2003) Phot-LOV1: photocycle of a blue-light receptor domain from the green alga *Chlamydomonas reinhardtii*. *Biophys J* **84**, 1192–1201.
  - 13 Song SH, Freddolino PL, Nash AI, Carroll EC, Schulten K, Gardner KH & Larsen DS (2011) Modulating LOV domain photodynamics with a residue alteration outside the chromophore binding site. *Biochemistry* **50**, 2411–2423.
  - 14 Song SH, Madsen D, van der Steen JB, Pullman R, Freer LH, Hellingwerf KJ & Larsen DS (2013) Primary photochemistry of the dark- and light-adapted states of the YtvA protein from *Bacillus subtilis*. *Biochemistry* **52**, 7951–7963.
  - 15 Swartz TE, Corchnoy SB, Christie JM, Lewis JW, Szundi I, Briggs WR & Bogomolni RA (2001) The photocycle of a flavin-binding domain of the blue light photoreceptor phototropin. *J Biol Chem* **276**, 36493–36500.
  - 16 Zhu J, Mathes T, Hontani Y, Alexandre MT, Toh KC, Hegemann P & Kennis JT (2016) Photoadduct formation from the FMN singlet excited state in the LOV2 domain of *Chlamydomonas reinhardtii* phototropin. *J Phys Chem Lett* **7**, 4380–4384.
  - 17 Arinkin V, Granzin J, Röllén K, Krauss U, Jaeger KE, Willbold D & Batra-Safferling R (2017) Structure of a LOV protein in apo-state and implications for construction of LOV-based optical tools. *Sci Rep* **7**, 42971.
  - 18 Salomon M, Christie JM, Knieb E, Lempert U & Briggs WR (2000) Photochemical and mutational analysis of the FMN-binding domains of the plant blue light receptor, phototropin. *Biochemistry* **39**, 9401–9410.
  - 19 Pudasaini A, Shim JS, Song YH, Shi H, Kiba T, Somers DE, Imaizumi T & Zoltowski BD (2017) Kinetics of the LOV domain of ZEITLUPE determine its circadian function in Arabidopsis. *Elife* **6**, e21646.
  - 20 Losi A, Polverini E, Quest B & Gärtner W (2002) First evidence for phototropin-related blue-light receptors in prokaryotes. *Biophys J* **82**, 2627–2634.
  - 21 Nakasone Y, Zikihara K, Tokutomi S & Terazima M (2010) Kinetics of conformational changes of the FKF1-LOV domain upon photoexcitation. *Biophys J* **99**, 3831–3839.
  - 22 Röllén K, Granzin J, Panwalkar V, Arinkin V, Rani R, Hartmann R, Krauss U, Jaeger KE, Willbold D & Batra-Safferling R (2016) Signaling states of a short blue-light photoreceptor protein PpSB1-LOV revealed from crystal structures and solution NMR spectroscopy. *J Mol Biol* **428**, 3721–3736.
  - 23 Röllén K, Granzin J, Batra-Safferling R & Stadler AM (2018) Small-angle X-ray scattering study of the kinetics of light-dark transition in a LOV protein. *PLoS One* **13**, e0200746.
  - 24 Conrad KS, Bilwes AM & Crane BR (2013) Light-induced subunit dissociation by a light-oxygen-voltage domain photoreceptor from *Rhodobacter sphaeroides*. *Biochemistry* **52**, 378–391.
  - 25 Vaidya AT, Chen CH, Dunlap JC, Loros JJ & Crane BR (2011) Structure of a light-activated LOV protein dimer that regulates transcription. *Sci Signal* **4**, ra50.
  - 26 Heintz U & Schlichting I (2016) Blue light-induced LOV domain dimerization enhances the affinity of Aureochrome 1a for its target DNA sequence. *Elife* **5**, e11860.
  - 27 Mansurova M, Scheerousse P, Simon J, Kluth M & Gärtner W (2011) Chromophore exchange in the blue light-sensitive photoreceptor YtvA from *Bacillus subtilis*. *ChemBioChem* **12**, 641–646.
  - 28 Krissinel E & Henrick K (2007) Inference of macromolecular assemblies from crystalline state. *J Mol Biol* **372**, 774–797.



- 29 Christie JM, Corchnoy SB, Swartz TE, Hokenson M, Han IS, Briggs WR & Bogomolni RA (2007) Steric interactions stabilize the signaling state of the LOV2 domain of phototropin 1. *Biochemistry* **46**, 9310–9319.
- 30 Zoltowski BD, Vaccaro B & Crane BR (2009) Mechanism-based tuning of a LOV domain photoreceptor. *Nat Chem Biol* **5**, 827–834.
- 31 Fedorov R, Schlichting I, Hartmann E, Domratcheva T, Fuhrmann M & Hegemann P (2003) Crystal structures and molecular mechanism of a light-induced signaling switch: the Phot-LOV1 domain from *Chlamydomonas reinhardtii*. *Biophys J* **84**, 2474–2482.
- 32 Möglich A & Moffat K (2007) Structural basis for light-dependent signaling in the dimeric LOV domain of the photosensor YtvA. *J Mol Biol* **373**, 112–126.
- 33 Sato Y, Nabeno M, Iwata T, Tokutomi S, Sakurai M & Kandori H (2007) Heterogeneous environment of the S-H group of Cys966 near the flavin chromophore in the LOV2 domain of Adiantum neochrome1. *Biochemistry* **46**, 10258–10265.
- 34 Zoltowski BD & Crane BR (2008) Light activation of the LOV protein vivid generates a rapidly exchanging dimer. *Biochemistry* **47**, 7012–7019.
- 35 Bolognesi M, Ghisla S & Incoccia L (1978) Crystal and molecular-structure of 2 models of catalytic Flavo(Co) enzyme intermediates. *Acta Crystallogr B* **34**, 821–828.
- 36 Conrad KS, Manahan CC & Crane BR (2014) Photochemistry of flavoprotein light sensors. *Nat Chem Biol* **10**, 801–809.
- 37 Alexandre MT, Arents JC, van Grondelle R, Hellingwerf KJ & Kennis JT (2007) A base-catalyzed mechanism for dark state recovery in the *Avena sativa* phototropin-1 LOV2 domain. *Biochemistry* **46**, 3129–3137.
- 38 Zayner JP & Sosnick TR (2014) Factors that control the chemistry of the LOV domain photocycle. *PLoS One* **9**, e87074.
- 39 Chan RH & Bogomolni RA (2012) Structural water cluster as a possible proton acceptor in the adduct decay reaction of oat phototropin 1 LOV2 domain. *J Phys Chem B* **116**, 10609–10616.
- 40 Rani R, Jentzsch K, Lecher J, Hartmann R, Willbold D, Jaeger KE & Krauss U (2013) Conservation of dark recovery kinetic parameters and structural features in the pseudomonadaceae "short" light, oxygen, voltage (LOV) protein family: implications for the design of LOV-based optogenetic tools. *Biochemistry* **52**, 4460–4473.
- 41 Losi A, Ghiraldelli E, Jansen S & Gärtner W (2005) Mutational effects on protein structural changes and interdomain interactions in the blue-light sensing LOV protein YtvA. *Photochem Photobiol* **81**, 1145–1152.
- 42 Pudasaini A, El-Arab KK & Zoltowski BD (2015) LOV-based optogenetic devices: light-driven modules to impart photoregulated control of cellular signaling. *Front Mol Biosci* **2**, 18.
- 43 Kawano F, Aono Y, Suzuki H & Sato M (2013) Fluorescence imaging-based high-throughput screening of fast- and slow-cycling LOV proteins. *PLoS One* **8**, e82693.
- 44 Raffelberg S, Mansurova M, Gärtner W & Losi A (2011) Modulation of the photocycle of a LOV domain photoreceptor by the hydrogen-bonding network. *J Am Chem Soc* **133**, 5346–5356.
- 45 Zoltowski BD, Nash AI & Gardner KH (2011) Variations in protein-flavin hydrogen bonding in a light, oxygen, voltage domain produce non-Arrhenius kinetics of adduct decay. *Biochemistry* **50**, 8771–8779.
- 46 Hart JE, Sullivan S, Hermanowicz P, Petersen J, Diaz-Ramos LA, Hoey DJ, Labuz J & Christie JM (2019) Engineering the phototropin photocycle improves photoreceptor performance and plant biomass production. *Proc Natl Acad Sci USA* **116**, 12550–12557.
- 47 Cao Z, Buttani V, Losi A & Gärtner W (2008) A blue light inducible two-component signal transduction system in the plant pathogen *Pseudomonas syringae* pv. *tomato*. *Biophys J* **94**, 897–905.
- 48 von Stetten D, Giraud T, Carpentier P, Sever F, Terrien M, Dobias F, Juers DH, Flot D, Mueller-Dieckmann C, Leonard GA *et al.* (2015) In crystallo optical spectroscopy (icOS) as a complementary tool on the macromolecular crystallography beamlines of the ESRF. *Acta Crystallogr D Biol Crystallogr* **71**, 15–26.
- 49 Flot D, Mairs T, Giraud T, Guijarro M, Lesourd M, Rey V, van Brussel D, Morawe C, Borel C, Hignette O *et al.* (2010) The ID23-2 structural biology microfocus beamline at the ESRF. *J Synchrotron Radiat* **17**, 107–118.
- 50 Bourenkov GP & Popov AN (2010) Optimization of data collection taking radiation damage into account. *Acta Crystallogr D Biol Crystallogr* **66**, 409–419.
- 51 Kabsch W (2010) Xds. *Acta Crystallogr D Biol Crystallogr* **66**, 125–132.
- 52 Winn MD, Ballard CC, Cowtan KD, Dodson EJ, Emsley P, Evans PR, Keegan RM, Krissinel EB, Leslie AG, McCoy A *et al.* (2011) Overview of the CCP4 suite and current developments. *Acta Crystallogr D Biol Crystallogr* **67**, 235–242.
- 53 Kantardjieff KA & Rupp B (2003) Matthews coefficient probabilities: improved estimates for unit cell contents of proteins, DNA, and protein-nucleic acid complex crystals. *Protein Sci* **12**, 1865–1871.
- 54 Adams PD, Afonine PV, Bunkoczi G, Chen VB, Davis IW, Echols N, Headd JJ, Hung LW, Kapral GJ, Grosse-Kunstleve RW *et al.* (2010) PHENIX: a comprehensive Python-based system for macromolecular structure solution. *Acta Crystallogr D Biol Crystallogr* **66**, 213–221.

- 55 Emsley P & Cowtan K (2004) Coot: model-building tools for molecular graphics. *Acta Crystallogr D Biol Crystallogr* **60**, 2126–2132.
- 56 Crosson S & Moffat K (2002) Photoexcited structure of a plant photoreceptor domain reveals a light-driven molecular switch. *Plant Cell* **14**, 1067–1075.
- 57 Lindorff-Larsen K, Piana S, Palmo K, Maragakis P, Klepeis JL, Dror RO & Shaw DE (2010) Improved side-chain torsion potentials for the Amber ff99SB protein force field. *Proteins* **78**, 1950–1958.
- 58 Beauchamp KA, Lin YS, Das R & Pande VS (2012) Are protein force fields getting better? A systematic benchmark on 524 diverse NMR measurements. *J Chem Theory Comput* **8**, 1409–1414.
- 59 Sousa da Silva AW & Vranken WF (2012) ACPYPE - AnteChamber PYthon Parser interface. *BMC Res Notes* **5**, 367.
- 60 Essmann U, Perera L, Berkowitz ML, Darden T, Lee H & Pedersen LG (1995) A Smooth Particle Mesh Ewald Method. *J Chem Phys* **103**, 8577–8593.
- 61 Humphrey W, Dalke A & Schulten K (1996) VMD: visual molecular dynamics. *J Mol Graph* **14**, 33–38.
- 62 Pettersen EF, Goddard TD, Huang CC, Couch GS, Greenblatt DM, Meng EC & Ferrin TE (2004) UCSF Chimera—a visualization system for exploratory research and analysis. *J Comput Chem* **25**, 1605–1612.
- 63 Kraulis PJ (1991) Molscript - a program to produce both detailed and schematic plots of protein structures. *J Appl Crystallogr* **24**, 946–950.
- 64 Merritt EA & Bacon DJ (1997) Raster3D: photorealistic molecular graphics. *Methods Enzymol* **277**, 505–524.
- 65 Kabsch W & Sander C (1983) Dictionary of protein secondary structure - pattern-recognition of hydrogen-bonded and geometrical features. *Biopolymers* **22**, 2577–2637.
- 66 Williams T & Kelley C (1986) Gnuplot 5.0: an interactive plotting program. [www.gnuplot.info](http://www.gnuplot.info)
- 67 Sievers F, Wilm A, Dineen D, Gibson TJ, Karplus K, Li W, Lopez R, McWilliam H, Remmert M, Soding J *et al.* (2011) Fast, scalable generation of high-quality

protein multiple sequence alignments using Clustal Omega. *Mol Syst Biol* **7**, 539.

## Supporting information

Additional supporting information may be found online in the Supporting Information section at the end of the article.

**Fig. S1.** Crystal packing of the PpSB2-LOV in (A) a-b plane and (B) in a-c plane showing solvent exposed C-termini. A single dimer is shown in blue and all other molecules in sand color. (C) The zoomed in view of panel B with a slight tilt ( $X = -10^\circ$ , and  $Y = -5^\circ$ ) for a better view. Bound FMN are shown as stick models and colored by element: carbon – yellow; nitrogen – blue; oxygen – red; phosphorus – purple.

**Fig. S2.** RMSD calculation for all residues, and only for the core residues (17–119) over the course of simulation with respect to the starting model. Each simulation run is depicted separately, red and magenta for all residues and blue and cyan for core residues.

**Table S1.** MD simulation data of PpSB2-LOV and PpSB1-LOV. We looked here for hydrogen bonding and salt-bridge formations. The data shows persistence of hydrogen bonds between partners in percentage of simulation time. As the proteins are dimers, the total time is 200%. Also shown are their conversions in nanoseconds.

**Table S2.** FMN-water interactions. Conservation in the interaction between chromophore and bound water molecules in LOV domains. Analysis of chromophore-bound water molecules in the structures of LOV domains listed in PDB database with a resolution of 2.0 Å and higher.

**Table S3.** FAD-water interactions. Conservation in the interaction between chromophore and bound water molecules in LOV domains. Analysis of chromophore-bound water molecules in the structures of LOV domains listed in PDB database with a resolution of 2.0 Å and higher.